



Since January 2020 Elsevier has created a COVID-19 resource centre with free information in English and Mandarin on the novel coronavirus COVID-19. The COVID-19 resource centre is hosted on Elsevier Connect, the company's public news and information website.

Elsevier hereby grants permission to make all its COVID-19-related research that is available on the COVID-19 resource centre - including this research content - immediately available in PubMed Central and other publicly funded repositories, such as the WHO COVID database with rights for unrestricted research re-use and analyses in any form or by any means with acknowledgement of the original source. These permissions are granted for free by Elsevier for as long as the COVID-19 resource centre remains active.



Imaging Features of Pediatric COVID-19 on Chest Radiography and Chest CT: A Retrospective, Single-Center Study

Zuhal Bayramoglu, MD, Eda Canipek, MD, Rana G. Comert, MD, Nilufar Gasimli, MD, Ozge Kaba, MD, Mehpare Sari Yanartaş, MD, Selda Hançerli Torun, Ayper Somer, Sukru Mehmet Erturk

Rationale and Objectives: This study aims to reveal the imaging features of Coronavirus Disease 2019 (COVID-19) in children.

Materials and Methods: Sixty-nine chest radiographs and 37 chest CT examinations of 74 children (36 male; median (interquartile range) age: 11 (6.25–15) years, 38 female; median (interquartile range) age: 12 (5.75–16) years) with positive real-time reverse transcription-polymerase chain reaction results between March 10 and May 31, 2020, were evaluated in this retrospective study. Differences in 0–<6, 6–<12, and 12–18 years of age groups were assessed with the Fisher's exact test or Kruskal-Wallis tests.

Results: Right-sided (3/69, 4.3%) or bilateral (3/69, 4.3%) ground-glass opacities without significant difference in age groups were depicted as radiographic findings related to COVID-19 in children. Opacities were either single (7/37, 18.9%) or bilateral (7/37, 18.9%) around the distal third of the bronchovascular bundle on CT. There was no significant difference in the median size of the largest opacities, total numbers of opacities and involved lobes, and the distance of the closest opacity to the pleura among age groups ($p > 0.05$). The rate of ground-glass opacities with or without consolidation (17/37, 45.94%) was higher than consolidation alone (6/37, 16.2%). Feeding vessel sign (16/37, 43.2%), halo sign (9/37, 24.3%), pleural thickening (6/37, 16.2%), interlobular interstitial thickening (5/37, 13.5%), and lymphadenopathy (3/37, 8.1%) were other imaging findings.

Conclusion: Unilateral or bilateral distributed ground-glass opacities often associated with feeding vessel sign, halo sign, and pleural thickening on chest CT without significant differences between age groups were findings of COVID-19 in children.

Key Words: Children; COVID-19; Lung; Radiography; CT.

© 2020 The Association of University Radiologists. Published by Elsevier Inc. All rights reserved.

Abbreviations: COVID-19 Coronavirus disease 2019, SARS-CoV-2 severe acute respiratory syndrome coronavirus 2, RT-PCR reverse transcription-polymerase chain reaction, CT computed tomography, GGO ground-glass opacity, PBT peribronchial thickening, IQR interquartile range, RUL right upper lobe, RML right middle lobe, RLL right lower lobe, LUL left upper lobe, LLL left lower lobe

INTRODUCTION

The SARS-CoV-2 is an enveloped and single-stranded RNA virus that is a member of the beta coronavirus family that has a zoonotic origin and causes “Coronavirus Disease 2019” (COVID-19) which may result in severe acute respiratory distress syndrome. SARS-CoV-2 is transmitted

through respiratory droplets of an infected person during coughing and sneezing, aerosols especially in crowded and poorly ventilated rooms, and less commonly contact with or touching contaminated surfaces. The virus has affected more than 29.4 million people, with more than 933,000 deaths worldwide as of September 15, 2020. The pediatric age group (<18 years) constituted 2572 (1.7%) of 149,082 diagnosed patients in early April in the United States with the infants (<1 year) accounting for 15% of pediatric COVID-19 cases (1). Asymptomatic infections are more frequent in children (2) probably due to lower frequencies of exposure to SARS-CoV-2 and less matured angiotensin-converting enzyme-2 receptors (3,4). Radiological examinations were less commonly required in children due to the lower overall incidences of infected, symptomatic, and severe cases in the pediatric age group compared to adults. The effects of the developing immune system on disease progression and imaging findings are still puzzling for pediatric COVID-19. SARS-CoV-2 may result in multisystem inflammatory syndrome in children associated with fever, severe illness, the

Acad Radiol 2021; 28:18–27

From the Radiology Department, Istanbul University, Istanbul Medical Faculty, Fatih, Millet Street, 34390, Istanbul, Turkey (Z.B., E.C., R.G.C., N.G., S.M.E.); Department of Pediatric Infectious Disease, Istanbul University, Istanbul Medical Faculty, Istanbul, Turkey (O.K., M.S.Y., S.H.T., A.S.). Received August 20, 2020; revised October 1, 2020; accepted October 1, 2020. The authors declare that they have all participated in the design, execution, and analysis of the paper, and they have approved the final version. Additionally, there are no conflicts of interest in connection with this paper, and the material described is not under publication or consideration for publication elsewhere. No financial support was taken during the paper was preparing. **Address correspondence to:** Z.B. e-mail: incezuhal@yahoo.com

© 2020 The Association of University Radiologists. Published by Elsevier Inc. All rights reserved.

<https://doi.org/10.1016/j.acra.2020.10.002>

TABLE 1. Median (IQR) Values of Age Parameters of Children with COVID-19 by Gender, Age Groups, and Radiological Examination Results

Parameters			Age (years) (Median (IQR))	<i>p</i>
All participants (n: 74)	Gender	Male (n: 36)	11 (6.25–15)	0.79
		Female (n: 38)	12 (5.75–16)	
	Age group (years)	0–<6 (n: 17)	3 (2–4)	0.001*
6–<12 (n: 22)		9 (8–10.25)		
12–18 (n: 35)		16 (14–17)		
Chest radiography examination (n: 69)	Findings	Normal (n: 56)	10 (5.25–14.75)	0.1
		Abnormal (n: 13)	10 (1.75–16)	
	Gender of the participant	Male (n: 32)	10 (4.25–14.75)	0.96
Female (n: 37)	10 (4–15)			
Chest CT examination (n: 37)	Findings	Normal (n: 18)	15 (9.5–16)	0.77
		Abnormal (n: 19)	13 (8.5–16.75)	
	Gender of the participants	Male (n: 18)	12.5 (8–15.5)	0.24
Female (n: 19)	15 (10–16)			

p-values were calculated by the Mann-Whitney U test / Kruskal Wallis test*.
IQR, interquartile range.

involvement of two or more organ systems in presence of increased inflammatory markers which may be caused by the postinfectious immune dysregulation. Transmission from children to older family members would be a critical problem for older family members owing to the reported higher frequency of severe illness. Additionally, the number of the affected children who are asymptomatic especially in the initial phases of the COVID-19 increases in the setting of family clusters (4,5).

Diagnostic tests for COVID-19 include the real-time reverse transcription-polymerase chain reaction (RT-PCR) testing from nasopharyngeal or throat swabs, IgM and IgG antibodies against SARS-CoV-2, and the radiological examinations, including chest radiography and chest computed tomography (CT). Chest CT examinations revealed high sensitivity (97%), relatively lower specificity (65%), and were found abnormal in the majority of adult patients (75%) who were initially tested negative by real-time RT-PCR (6). However, the Centers for Disease Control does not recommend radiological examinations as a specific method of COVID-19 diagnosis, and confirmation of COVID-19 by viral testing is crucial even if the radiological findings are suggestive of COVID-19 (7). Radiological manifestations of COVID-19 vary between age groups (8). A recent study (9) reviewed the studies investigating imaging characteristics of COVID-19 in children with a small sample size (10–14). In this article, we aimed to document the chest radiography and chest CT imaging findings of children with COVID-19 from a single academic center and to compare our results with the existing literature.

MATERIALS AND METHODS

Study Protocol and Patients

The present retrospective study was conducted at a single academic center (Istanbul University, Istanbul Medical Faculty,

Radiology Department) and included consecutive children each were diagnosed with COVID-19 by positive real-time RT-PCR tests between March 10 and May 31, 2020. Children with negative real-time RT-PCR results were excluded. The local ethics committee approved the study (file number: 86531). Informed consent was waived because of the retrospective nature of the study. None of the patients had a chronic cardiac, pulmonary, or hepatic disease that may lead to lymphadenopathy, pleural effusion, or pulmonary interlobular interstitial thickening which may mimic COVID-19 related findings. Real-time RT-PCR tests were evaluated in two laboratories under the supervision of the Ministry of Health and Istanbul Medical Faculty. A total of 74 children with a diagnosis of COVID-19 were included (Table 1). Chest radiographs of 69 children and chest CT examinations of 37 children) diagnosed with COVID-19 were reviewed. Patients were divided into 3 age groups: (A) 0–<6 years (median 3, interquartile range [IQR] 2–4) years, (B) 6–<12 years (median 9, IQR 8–10.25), and (C) 12–18 years (median 16, IQR 14–17). Chest radiographs were not available in five patients, owing to the being performed in external medical centers and referred to our tertiary care center.

Thirty-three children (median age [IQR]: 10 (6–15) years; male: 13, female: 19) had both chest CT and chest radiography examinations with a median interval of 0 days (IQR: 0–1 days) between examinations. Abnormal CT and radiographic imaging findings and the time interval between chest radiographs and chest CT examinations of pediatric patients with known real-time RT-PCR positivity were investigated retrospectively and consecutively by two radiologists (ZB, a pediatric radiologist with more than 9 years of radiology experience; EC, a radiologist having more than 3 years of radiology experience) who were blinded to the symptoms owing to the lack of the available systematic clinical information in the database.

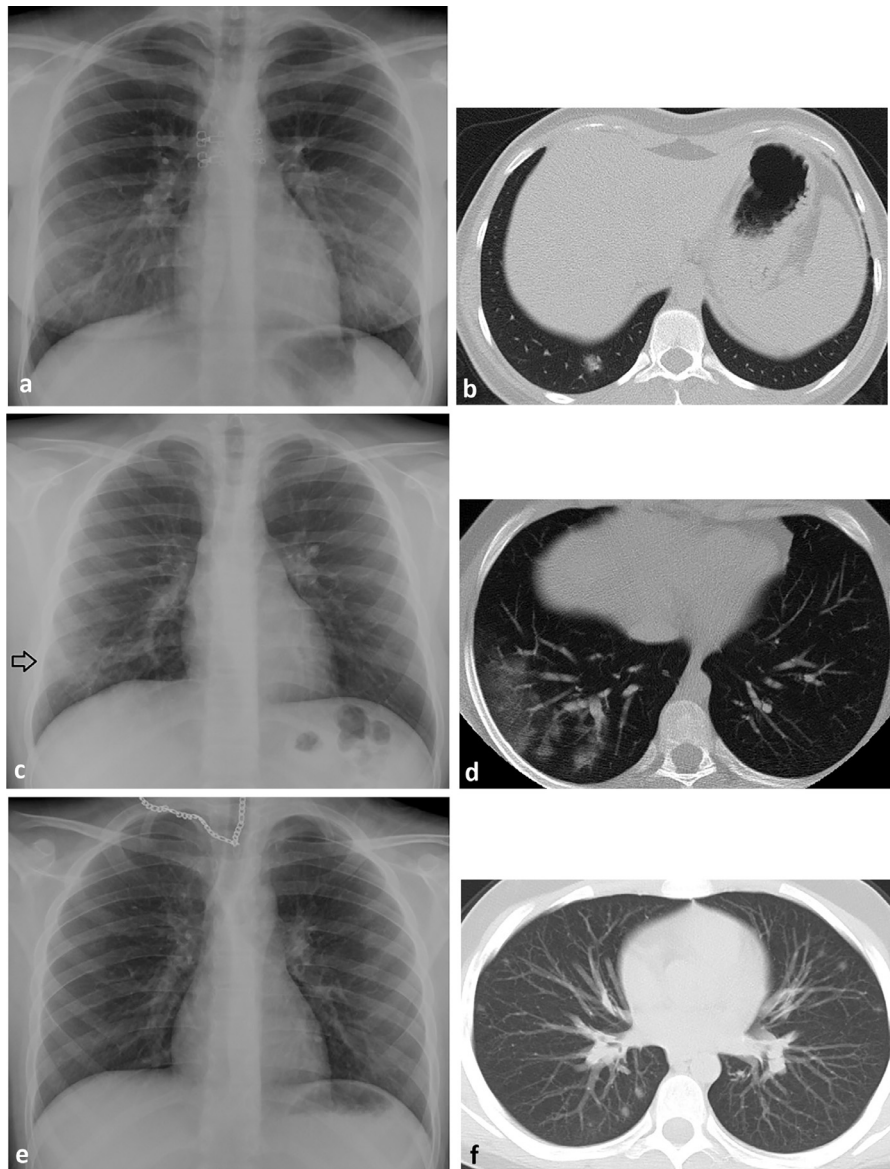


Figure 1. Chest radiography and chest CT findings of the children with COVID-19 in conjunction with symptom and time interval between imaging studies. (a, b) Imaging findings of a 13-year-old female patient with COVID-19. (a) Posteroanterior chest radiograph of a 13-year-old female patient presented with fever for 2 days. Chest radiography and chest CT images were obtained on the same day. The chest radiography was normal. (b) Chest CT image in the axial plan revealed a single, peripheral located, ground-glass opacity at the posterobasal segment of the right lower lobe. The opacity was obscured with the right liver lobe and diaphragm on chest radiography. (c, d) Imaging findings of a 10-year-old male patient with COVID-19. (c) Posteroanterior chest radiograph of a 10-year-old male patient presented with cough and fever for two days. Chest radiography and chest CT images were obtained on the same day. The chest radiography revealed peripheral ground-glass opacity (arrow) at the basal segments of the right lower lobe. (d) Axial section chest CT examination revealed bronchovascular distributed ground-glass opacities in a 10-year-old male patient at the periphery of the basal segments of the right lower lobe. (e, f) Imaging findings of a 13-year-old male patient with COVID-19. (e) Posteroanterior chest radiograph of a 13-year-old male patient presented with cough and fever for two days. Chest radiography and chest CT images were obtained on the same day. The chest radiography was interpreted as normal. (f) Axial chest CT image of the 13-year-old male patient without contrast demonstrates bilateral, multifocal, peripherally, and perivascular distributed millimetric nodular-shaped ground-glass opacities. The opacities were not detected on chest radiography due to the smaller size and lower density. (g, h) Imaging findings of a 16-year-old female patient with COVID-19. (g) Posteroanterior chest radiograph of the 16-year-old female patient presented with cough and fever for 3 days. Chest radiography and chest CT images were obtained on the same day. The chest radiography demonstrates paramediastinal ground-glass opacity at the right upper lobe (red frame). (h) Axial chest CT image of the 16-year-old female patient without contrast demonstrates peripherally distributed ground-glass opacity at the right upper lobe with an interlobular interstitial thickening. (i) Anteroposterior chest radiography of an intubated and a 15-year-old female patient presented with diarrhea and hypotension on the fourth day of fever, demonstrates diffusely distributed GGOs in the right lung in addition to left perihilar and basilar opacities. Right-sided pleural effusion (arrows) was also depicted. The patient was diagnosed with multisystem inflammatory syndrome associated with COVID-19 and she was the only patient that resulted in COVID-19 related pediatric death in our clinic. Laboratory examinations revealed lymphopenia ($6.64 \times 10^9/L$), thrombocytopenia ($94 \times 10^9/L$), elevated creatinine (1.24 mg/dL), troponin-T (37.45 pg/mL), PRO-BNP (5578 pg/mL), bilirubin (0.48 mg/dL), alanine transaminase (43.8 U/L), C-reactive protein (377 mg/L). (Color version of figure is available online.)

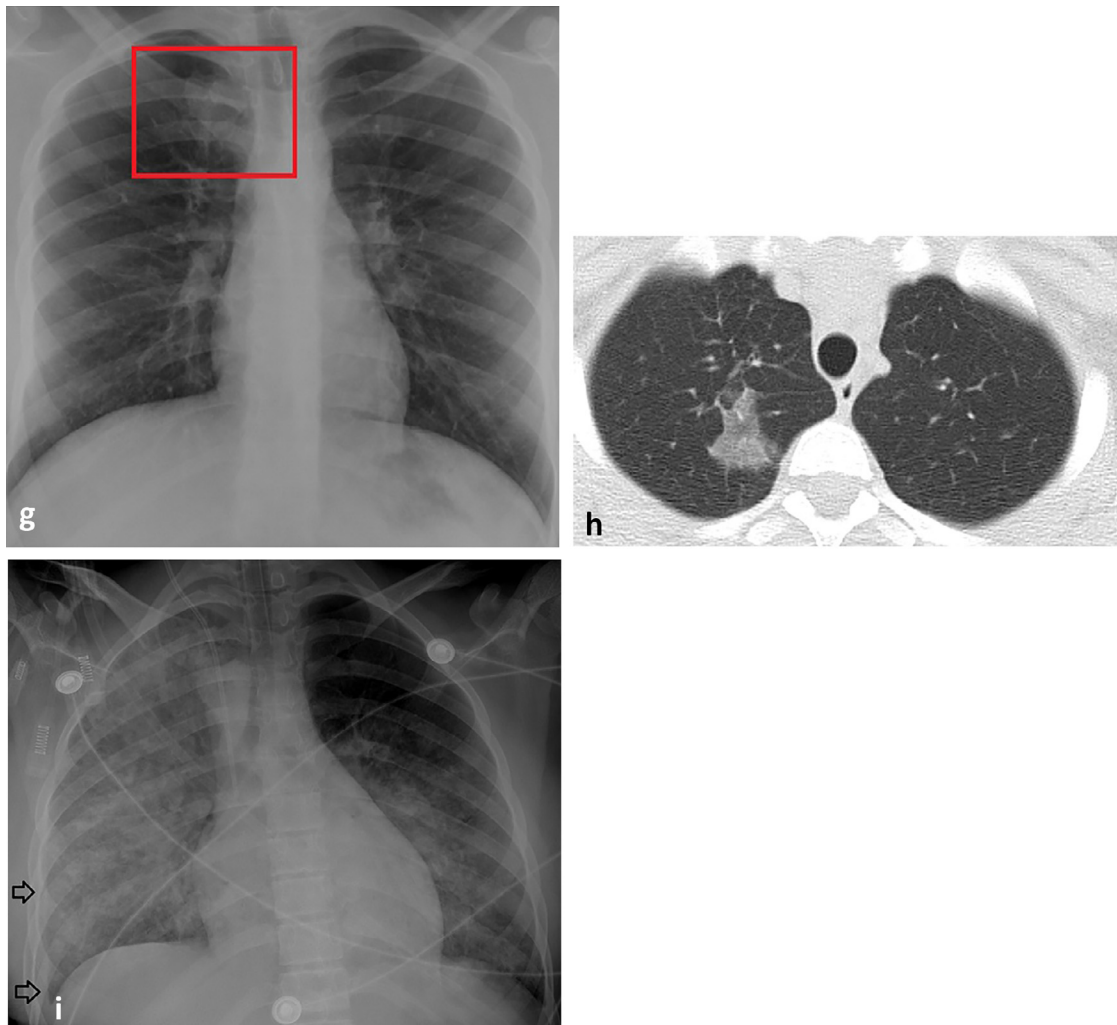


Figure 1 Continued.

Chest Radiography Examination

All examinations were obtained using a fixed X-ray device (Toshiba Rotanode E7869XX, Tochigi, Japan) reserved for the COVID-19 outbreak in the pandemic unit. Single view posteroanterior chest radiography examinations were performed in an erect posture with breath-hold in cooperative patients. Respiratory or motion artifacts preventing the evaluation were not observed on the radiographs of the patients who could not breathe hold. Therefore, all examinations were included for investigation. The exposure dose was adjusted based on the patient's age and weight, varying between 55kVp, 5 mAs, and 100 kVp, 100 mAs.

All radiographs were retrospectively searched from the database and evaluated consecutively for COVID-19 related imaging findings including peribronchial thickening (PBT), ground-glass opacities (GGOs), and consolidations (Fig 1), distribution of opacities (central or peripheral; unilateral or bilateral), number of the opacities, and associated abnormalities such as pleural effusion, and mediastinal or hilar lymphadenopathy according to the

recommendations by the Fleischner Society (15). The reasons for the lack of the detectability of COVID-19 on the chest radiographs were documented by comparing the abnormal chest CT findings of the patients with normal chest radiographs based on the location, distribution, size, and density of the opacities (Fig 2).

Chest CT Examination

Children with suspicious COVID-19 related symptoms and signs regarding cough, fever, diarrhea, hypotension, dyspnea, loss of taste and smell, and myalgia underwent chest CT examinations using a 64 detector CT scanner (Aquillon 64, Toshiba Medical Systems, Tochigi, Japan) without intravenous contrast. (Weight based tube voltage: 100–120 KV, reconstruction interval: 5, pitch: 0.65; slice thickness: 5 mm). Intravenous contrast agents are used to evaluate for complicated pneumonia with necrosis, vascular complications, and mediastinal enlargement in children in our department. None of the children with a suspect of COVID-19 were initially undergoing contrast-enhanced

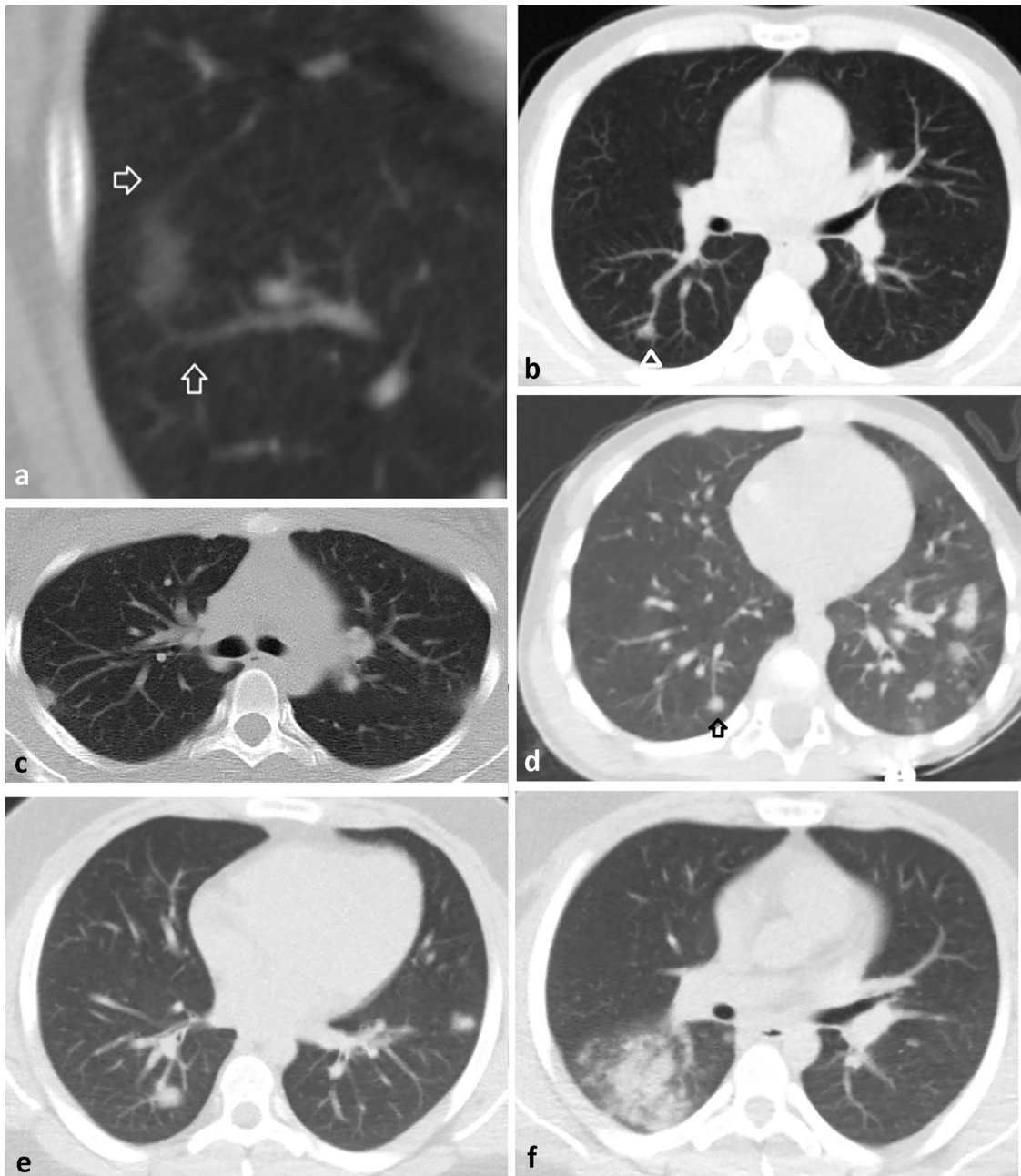


Figure 2. Chest CT findings of children with COVID-19. (a) Axial chest CT image of a 16-year-old male patient without contrast on the 2nd day of fever and cough shows a single, peripheral ground-glass opacity and bridging vessels (arrows) around the ground-glass opacity at the laterobasal segment of the right lower lobe. The continuous vessels at the peripheral vascular network around the opacity may suggest angio-centric inflammation. (b) Axial chest CT image of an 11-year-old male patient without contrast was performed one day after fever and cough onset. CT image demonstrates a nodule (arrowhead) with well-defined margins located in the pulmonary artery bifurcation of the upper segment of the right lower lobe with a feeding vessel sign without vascular enlargement. (c) Axial chest CT image of a 16-year-old female patient without contrast was performed one day after fever and cough onset. The image reveals multifocal peripheral-subpleural consolidations with halo sign. (d) Axial chest CT image of a 3-year-old male patient was performed without contrast six days after fever and cough onset. The chest CT image shows bilateral, multifocal, and perivascular distributed round-shaped consolidations without halo sign. Note the feeding vessel signs (arrow). (e, f) Chest CT imaging findings of a 17-year-old male patient with COVID-19. (e) Axial CT image of the chest without contrast performed five days after fever and cough onset of a 17-year-old male patient reveals bilateral nodular-shaped consolidations. (f) Axial CT image of the chest without contrast performed five days after fever and cough onset of the 17-year-old male patient reveals bronchovascular distributed consolidations with halo sign and centrilobular ground-glass opacities at the right lower lobe.

chest CT. Cooperative patients were asked to hold their breath. All chest CT images were reviewed according to the recommendations by the Fleischner Society (15). Findings compatible with chronic sequelae such as air trapping due to bronchial atresia, calcific nodules, or calcific lymph nodes were described as irrelevant imaging findings for COVID-19. Findings other than those in children with COVID-19 were classified according to age groups.

COVID-19 related imaging findings included pulmonary opacities (either as GGO or consolidation), pulmonary nodules (except for calcific or noninfectious interstitial nodules), pleural and interlobular septal thickening, lymph nodes (short-axis diameter greater than 10 mm), and pleural effusion on chest CT were noted in each patient. Distribution of the opacities in the lung lobes and around the proximal, middle, or distal third of the bronchovascular bundles was noted. The total number of the involved lobes and opacities were calculated. Distribution was categorized as single, multiple (in a lung or a lobe), and bilateral. The largest dimension of the largest opacity and the distance of the closest opacity to the pleura were measured. The involvement pattern (nodular or peribronchial), margins (well-defined or ill-defined), density category of the opacities, presence of associated imaging findings (feeding vessel sign, halo sign, air bronchogram, tree-in-bud sign, atoll sign, diffuse GGOs or consolidative opacities, crazy paving, pleural thickening, presence of lymphadenopathy, and pleural effusion) were reviewed. The suspicion level of COVID-19 infection based on the CT imaging findings in adults has been proposed by several COVID-19 imaging reporting and data systems such as COVID-RADS (COVID-RADS 0, normal chest CT, COVID-RADS 1, low suspicion, COVID-RADS 2, moderate suspicion, and COVID-RADS 3, high suspicion levels) and CO-RADS (CO-RADS 1, normal chest CT or noninfectious findings, CO-RADS 2 low suspicion level, typical for infections other than COVID-19, CO-RADS 3, equivocal, features compatible with COVID-19 and also other diseases, CO-RADS 4, high suspicion level for COVID-19, CO-RADS 5, very high suspicion level,

typical for COVID-19, CO-RADS 6, RT-PCR positive for SARS-CoV-2). We categorized the findings to reveal suspicion levels of COVID-19 related imaging findings in children based on suggestions of the recent literature for adults as COVID-RADS (16), CO-RADS (17) except for CO-RADS 6 corresponding to known real-time RT-PCR positivity, and Radiological Society of North America Expert Consensus Statement (18).

Statistical Analysis

The statistical analysis was performed using the Statistical Package for the Social Sciences (SPSS; version 21, IBM Corp.). Categorical variables were expressed as a percentage (%) and assessed using Fisher's exact test to compare 0–<6 years vs 6–<12 years, 6–<12 years vs 12–18 years, and 0–<6 years vs 12–18 years of age groups. Nonparametric quantitative data were expressed as median (IQR) and compared with the Kruskal-Wallis test among age groups. Spearman's correlation analysis was performed to assess the association of quantitative data. A *p* value of less than 0.05 is considered statistically significant.

RESULTS

The descriptive statistics related to gender, age groups, and test results of the patients are given in Table 1. No statistically significant differences were found regarding the ages of the patients based on gender (*p* = 0.79), chest radiography (*p* = 0.1), and chest CT findings (*p* = 0.77).

Chest radiography examination results are given in Table 2. Abnormal findings on chest radiography were depicted in 18.8% (13/69) of the patients, 6 in 0–<6 years, 1 in 6–<12 years, and 6 in the 12–18 years of age groups. No significant differences were found regarding unilateral or bilateral involvement, numbers of opacities, and central or peripheral distribution by age groups (*p* = 1). PBT was seen

TABLE 2. Chest Radiography Findings of 69 Children Diagnosed with COVID-19 by Positive Real Time RT-PCR Tests

Parameter	0–<6 years (n: 20)			6–<12 years (n: 23)			12–18 years (n: 26)			<i>p</i>
	Number (Percentage, %)			Number (Percentage, %)			Number (Percentage, %)			
Number of patients with abnormalities	6 (30)			1 (4.3)			6 (23)			0.9
Location of opacity	Right	1 (5)		0		2 (7.6)		1		
	Left	0		0		0				
	Bilateral	1 (5)		0		2 (7.6)				
Numbers of opacities	Single	0		0		2 (7.6)		1		
	Multiple	2 (10)		0		2 (7.6)				
Distribution	Central	1 (5)		0		2 (7.6)		1		
	Peripheral	1 (5)		0		2 (7.6)				
	GGO	2 (10)		0		3 (11.5)				
Pleural effusion	0			0			1 (3.8)			1
PBT	6 (30)			1 (4.3)			0			0.8

p values were calculated for comparison of the groups; 0–<6 years vs 6–<12 years, 6–<12 years vs 12–18 years, and 0–<6 years vs 12–18 years by the Fisher's exact test.

GGO, ground-glass opacity; PBT, peribronchial thickening.

TABLE 3. Chest CT Evaluation Results Based on Location, Size, and Distribution of COVID-19 Related Imaging Findings in Children by Three Age Groups

Parameter		0–<6 years (n: 3) Number (Percentage, %)/ Median (IQR)	6–<12 years (n: 10) Number (Percentage, %)/ Median (IQR)	12–18 years (n: 24) Number (Percentage, %)/ Median (IQR)	<i>p</i>
Involved lobes	RUL - RML	2 (0.66)	3 (0.3)	8 (0.33)	Lower vs middle-upper: 1' 0.55''
	RLL	1 (0.33)	3 (0.3)	6 (0.25)	
	LUL/LLL	1 (0.33)/2 (0.66)	1(0.1)/0	4 (0.16)/6 (0.25)	
	Total number	3 (1–4)	1 (1–2)	2 (1–3.25)	
Distribution	Single opacity	1 (0.33)	2 (0.2)	4 (0.16)	Single vs multiple-bilateral: 0.85' Distal vs proximal-middle: 1'
	Multiple	0	2 (0.2)	2 (0.08)	
	Bilateral	1 (0.33)	1 (0.1)	5 (0.21)	
	Proximal - Middle	1 (0.33)	1 (0.1)	3 (0.12)	
	Distal	2 (0.66)	5 (0.5)	10 (0.41)	
Largest opacity size (mm)		30 (4–44)	8 (4.5–58)	7.5 (4.75–14)	0.86''
Total opacity number		14 (1–20)	2 (1–4.5)	2 (1–7.5)	0.73''
Distance to the pleura (mm)		1 (0–2)	0 (0–2)	0 (0–2.8)	0.53''

p values for comparison of categorical parameters of the groups 0–<6 years vs 6–<12 years, 6–<12 years vs 12–18 years, and 0–<6 years vs 12–18 years of age were obtained by the ' Fisher's exact test. The smallest *p* value was given for each descriptor. *p* values for comparison of quantitative parameters of the age groups were obtained by the "Kruskal Wallis test."

IQR, interquartile range; LLL, left lower lobe; LUL, left upper lobe; RLL, right lower lobe; RML, right middle lobe; RUL, right upper lobe.

in 7 patients in the 0–<12 years of age group and GGOs were seen in 2 patients in the 0–6 year age group and in 3 patients in the 12–18 year age group ($p = 0.02$). Pleural effusion was encountered in only 1 patient (1/69, 1.4%), in the 12–18 year age group.

The interval from the symptom onset to chest CT examinations was 2 ± 1.4 days (median [IQR]: 2 [1–3] days). Most of the patients (30/37, 81%) with CT examination were in the first 4 days of the symptoms corresponding to early stage, and 19% (7/37) were in the progressive stage.

Chest CT examination results based on distribution and quantitative CT parameters are given in Table 3. Abnormalities were depicted in 2 of 3 patients in the 0–<6 years, 6 of 10 patients in 6–<12 years, and 11 of 24 patients in the 12–18 years of age groups. Location at the lower lobes (18/37, 48.65%) and around 1/3 distal to the bronchovascular bundles (17/37, 45.9%) were depicted distributions of COVID-19 related opacities in children. Opacities were sometimes single (7/37, 18.9%) or distributed bilaterally (7/37, 18.9%). There were no significant differences between age groups in the median values of the total number of opacities ($p = 0.73$) and involved lobes ($p = 0.55$), size ($p = 0.86$) of the largest opacity, the distance of the closest opacity to the pleura ($p = 0.53$).

Chest CT examination results based on the shape and density of the COVID-19 related imaging findings are given in Table 4. Opacity pattern was identified either as peribronchial type (12/37, 32.4%) or as nodular (12/37, 32.4%) type. The rate of GGOs with or without consolidation (17/37, 45.9%) was higher than consolidations with or without halo sign (6/37, 16.2%). The opacity margins were sometimes ill-defined (16/37, 43.2%). Feeding vessel sign (16/37, 43.2%), halo sign

(9/37, 24.3%), pleural thickening (6/37, 16.2%), interlobular interstitial thickening (5/37, 13.5%), and lymphadenopathy (3/37, 8.1%) were other imaging findings. Tree-in-bud sign, atoll sign, and diffuse GGOs and consolidative opacities were not observed.

Scores by CO-RADS, COVID-RADS, and Radiological Society of North America Expert Consensus Statement are given in Table 5. CO-RADS scores over three were depicted in 29.7% (11/37) of the cases (CO-RADS 4: 10.8% [4/37] and CO-RADS 5: 18.9% [7/37]), and COVID-RADS score 3 was found in 8 of 37 (21.6%) cases. The typical appearance of COVID-19 based on RSNA expert consensus statement was depicted in 21.6% (8/37) of the cases (Supplemental Tables 1–3).

There were statistically significant positive correlations among the total number of opacities with the total number of involved lobes ($p = 0.001$, $r = 0.91$) and the largest opacity size ($p = 0.038$, $r = 0.52$). The distance of the closest opacity to the pleura decreases with increased opacity numbers without statistical significance ($p = 0.07$, $r = -0.47$).

DISCUSSION

We investigated the imaging findings of pediatric COVID-19 on chest radiography and chest CT with a detailed classification. Imaging findings were compared among three different age groups. Findings on CT were lower lobe predominant, peripherally distributed, single or bilateral GGOs. The distinctive CT findings were feeding vessel sign, halo sign, and pleural thickening. Scores on the systems developed for adults were mostly corresponding to low suspicion level.

TABLE 4. Opacity Patterns of COVID-19 Related Imaging Findings in Children by Age Groups on Chest CT

Parameter	0–<6 years (n: 3)	6–12 years (n: 10)	12–18 years (n: 24)	<i>p</i>	
	Number (Percentage, %)	Number (Percentage, %)	Number (Percentage, %)		
Abnormal findings	2 (0.66)	6 (0.6)	11 (0.46)	0.4	
Opacity pattern	Nodular	2 (0.66)	3 (0.3)	7 (0.29)	0.6
	Peribronchial	1 (0.33)	3 (0.3)	8 (0.33)	
Margin	Well-defined	1 (0.33)	1 (0.1)	2 (0.08)	0.53
	Ill-defined	1 (0.33)	4 (0.4)	11 (0.46)	
Opacity density	GGO	1 (0.33)	3 (0.3)	6 (0.25)	GGO vs consolidation: 0.52
	GGO + consolidation (<50%)	0	1 (0.1)	4 (0.16)	
	GGO + consolidation (>50%)	0	0	2 (0.08)	
	Consolidation	1 (0.33)	1 (0.1)	4 (0.16)	
Associated findings	Obscured vessels	2 (0.66)	2 (0.2)	1 (0.04)	0.55
	Feeding vessel sign	2 (0.66)	5 (0.5)	9 (0.37)	0.57
	Halo sign	1 (0.33)	2 (0.2)	6 (0.25)	0.64
	Air bronchogram	1 (0.33)	0	0	0.4
	Lymphadenopathy	1 (0.33)	1 (0.1)	1 (0.04)	0.53
	Pleural thickening	0	2 (0.2)	4 (0.16)	0.43
	Interlobular interstitial thickening	1 (0.33)	2 (0.2)	2 (0.08)	0.58

p values for comparison of categorical parameters of the groups 0–<6 years vs 6–<12 years, 6–<12 years vs 12–18 years, and 0–<6 years vs 12–18 years of age were obtained by the Fisher's exact test. Because all comparisons were not statistically significant, the smallest *p* value was given for each descriptor.

GGO, ground-glass opacity.

TABLE 5. Categories of the Chest CT Findings Based on Classification Systems and Different Age Groups

Classification	0–<6 years (n: 3)	6–<12 years (n: 10)	12–18 years (n: 24)	Total (n: 37)	
	Number (Percentage, %)	Number (Percentage, %)	Number (Percentage, %)	Number (Percentage, %)	
RSNA expert consensus statement	Typical appearance	1 (0.33)	2 (0.2)	5 (0.21)	8 (21.6)
	Indeterminate appearance	1 (0.33)	2 (0.2)	2 (0.08)	5 (13.5)
	Atypical appearance	0	2 (0.2)	3 (0.12)	5 (13.5)
	Negative for pneumonia	1 (0.33)	4 (0.4)	14 (0.58)	19 (51.3)
COVID-RADS	0 - Low suspicion	1 (0.33)	5 (0.5)	12 (0.5)	18 (48.6)
	1 - Low suspicion	0	0	3 (0.12)	3 (8.1)
	2A - Moderate	1 (0.33)	3 (0.3)	3 (0.12)	7 (18.9)
	2B - Moderate	0	0	1 (0.04)	1 (2.7)
	3 - High	1 (0.33)	2 (0.2)	5 (0.21)	8 (21.6)
CO-RADS	0 - Not interpretable	0	0	0	0
	1 - Very low	1 (0.33)	5 (0.5)	12 (0.5)	18 (48.6)
	2 - Low	0	0	3 (0.12)	3 (8.1)
	3 - Equivocal/Unsure	1 (0.33)	2 (0.2)	2 (0.08)	5 (13.5)
	4 - High	0 (0.33)	1 (0.1)	3 (0.12)	4 (10.8)
5 - Very high	1 (0.33)	2 (0.2)	4 (0.16)	7 (18.9)	

Real-time RT-PCR is the gold standard in the diagnosis of COVID-19 and is recommended in symptomatic patients (19). However, children in the initial phases of the COVID-19 may be asymptomatic but can cause the spread of COVID-19 to family members. Due to the lack of apparent abnormalities in routine blood and other laboratory tests in a considerable number of

children, low-dose CT examination would be a diagnostic tool only in high-prevalence environments in which there is no appropriate access to viral testing. Thus, the transmission of SARS-CoV-2 to the family members or vulnerable pediatric patients may be reduced in that manner (20). Children with positive real-time RT-PCR results may be asymptomatic in up to

one-third with negative imaging findings, but a considerable number of patients (43/50, 86%) were positive on CT investigation (21). Being aware of COVID-19 related patterns on CT examination would be discriminatory in selected cases to decide whether to admit children into the SARS-CoV-2 free service or a pandemic service. However, the opacity patterns were found to be subtle and different when compared to adults. The depicted CT positivity ratio in the current study (19/37, 51.3%) was considerably higher than a recent study reported normal CT studies in 77% of 30 children (11). However, the depicted CT positivity ratio (51.3%) was still insufficient to distinguish pediatric COVID-19 cases reliably. CT examinations should not be a screening tool for pediatric COVID-19 diagnosis owing to the frequently mild or moderate clinical courses of the pediatric COVID-19 cases, less commonly encountered findings with high suspicion of COVID-19, as well as the negative aspects of the radiation exposure (22). On the other hand, there has been an identified real-time RT-PCR negative but a radiologically positive group with definite SARS-CoV-2 exposure (21). Because real-time RT-PCR test results are affected by sampling operations and timing owing to the cycle thresholds in the sources (6).

In this analysis, the majority of the causes for normal-appearing chest radiographs for COVID-19 while there have been positive findings on the chest CT were due to low-density opacities (7/23, 30%), small-sized opacities (6/23, 26%), or basal-located opacities obscured with the diaphragm and hepatic dome on posteroanterior chest radiography (4/23, 17%). Chest radiography findings of COVID-19 were GGOs and/or PBT. PBT is unusual for adult COVID-19 findings (23) but typical for viral pneumonia in children. Abnormal findings in children with the severe acute respiratory syndrome have been reported to be multifocal in one-third of cases with unilateral and lower zone predominance in the early phase (24). Coronavirus-borne diseases as SARS or SARS-CoV-2 may be depicted in a small number of children by radiographs.

SARS-CoV-2 causes acute respiratory distress syndrome due to diffuse alveolar hemorrhage, diffuse intravascular coagulation, intussusceptive angiogenesis (25), and nearly total occlusion of vessels by complement associated thrombosis (26). Opacities were generally closer than 2 mm to the pleura suggesting that their peripheral distributions are related to the involvement of small-sized pulmonary vessels. The low-density opacities as GGOs are corresponding to a hyaline membrane, and pulmonary edema in 97% and presence of alveolar hemorrhage in 87% of the cases (27,28). The feeding vessels disclose angiocentric inflammation. Pulmonary blood vessels are thinner in children, and changes in size may be subtle due to respiratory artifacts and section thickness. Although vascular enlargement was not common in the pediatric cases, the “feeding vessels” passing through the central part of the nodules or peribronchial opacities with a higher density compared to the intact section would be apparent and easy to detect the angiocentric inflammation as an observational parameter and alternative sign for vascular enlargement. Additionally, multiple feeding arteries around peripheral - subpleural opacity may be entitled “bridging vessels” and may also

strengthen the angiocentric inflammation at the peripheral pulmonary vascular network.

There has been a peripheral and lower lobe predominant distribution pattern with bilateral numerous opacities in our pediatric cohort, similar to previous studies (11,21). There is no available data in the literature in terms of the total number of the opacities and the distance of COVID-19 related opacities to the pleura in the children. We described GGOs or consolidations in 51.3% of our cohort with the GGOs presenting a higher rate without a significant difference between age groups. A predominant GGO pattern (8,11,22,26,29) followed by a GGO pattern accompanied by consolidations (8,14,30,31) and consolidations alone (32) were depicted in several studies. A higher incidence of consolidations with or without halo sign compared to GGOs with or without consolidations was also reported in a recent study (32). The density pattern of the opacities would depend on the stage of the disease. The surrounding halo sign is commonly associated with segmental consolidations (14). PBT is uncommon in the adult population and nonspecific for COVID-19 but is depicted in children with COVID-19 (12). On the other hand, interlobular septal thickening associated with GGOs (5/37, 13.5%) were less frequently depicted compared to adults. Nodular shaped consolidations and perivascular distributed nodules were not noted in the adult population. We demonstrated a nodular pattern in one of three children (32.4%) compatible with the literature (11,12,26,31). The halo sign (11) detection ratio was lower than the previous study, which included a smaller sample size. Most of the patients did not score high on the new scoring systems adjusted for adults. Therefore, these scoring systems seem to be not applicable to children. Although given a higher number of participants with positive COVID-19 related imaging findings, this population is still insufficient to reveal a common lexicon for COVID-19 radiological evaluation in the pediatric population due to heterogeneous opacity patterns. Therefore, a modified scoring system adapted for children is needed based on vascular and perivascular changes.

This study has some limitations. First, superimposed or concomitant pneumonia due to different infectious agents was not excluded via laboratory tests because of the restricted viral respiratory panel tests in our laboratory owing to the real-time RT-PCR test load due to the COVID-19 pandemic. Second, although this study frequently reflects the early imaging findings of pediatric COVID-19, most of patients were in the early phases of the disease, and opacity characteristics may change over time, especially in the progressive stage.

In conclusion, pediatric COVID-19 related imaging findings may be subtle both on chest radiography and also chest CT examinations. Imaging findings reveal different and heterogeneous opacity patterns compared to adults. The findings of pediatric COVID-19 can be handled in different categories than those defined for adults. In symptomatic cases, pediatric COVID-19 awareness can be created by the described findings until the real-time RT-PCR results are obtained. Given the negative aspects of radiation exposure, higher incidence

of indeterminate appearances of COVID-19 related imaging findings in children, chest CT examinations are not essential in the diagnosis of pediatric COVID-19.

REFERENCES

- Covid C, Covid C, Covid C, et al. Coronavirus disease 2019 in children—United States, February 12–April 2, 2020. *Morbidity and Mortality Weekly Report* 2020; 69(14):422.
- Wu Z, McGoogan JM. Characteristics of and important lessons from the coronavirus disease 2019 (COVID-19) outbreak in China: summary of a report of 72 314 cases from the Chinese Center for Disease Control and Prevention. *Jama* 2020; 323(13):1239–1242.
- Dong Y, Mo X, Hu Y, et al. Epidemiology of COVID-19 among children in China. *Pediatrics* 2020; 145(6). doi:10.1542/peds.2020-0702.
- Chan JF, Yuan S, Kok KH, et al. A familial cluster of pneumonia associated with the 2019 novel coronavirus indicating person-to-person transmission: a study of a family cluster. *Lancet (London, England)* 2020; 395(10223):514–523. doi:10.1016/s0140-6736(20)30154-9.
- An P, Zhang M. Novel coronavirus SARS-CoV-2: familial spread resulting in COVID-19 pneumonia in a pediatric patient. *Diagn Intervent Radiol (Ankara, Turkey)* 2020; 26(3):262–263. doi:10.5152/dir.2020.20157.
- Ai T, Yang Z, Hou H, et al. Correlation of chest CT and RT-PCR testing in coronavirus disease 2019 (COVID-19) in China: a report of 1014 cases. *Radiology* 2020;200642doi:10.1148/radiol.20200642.
- ACR recommendations for the use of chest radiography and computed tomography (CT) for suspected covid-19 infection. American College of Radiology website. <https://www.acr.org/Advocacy-and-Economics/ACR-Position-Statements/> Published March 11, 2020. Updated March 22, 2020.
- Chen Z, Fan H, Cai J, et al. High-resolution computed tomography manifestations of COVID-19 infections in patients of different ages. *Eur J Radiol* 2020; 126:108972. doi:10.1016/j.ejrad.2020.108972.
- Katal S, Johnston S, Johnston J, et al. Imaging findings of SARS-CoV-2 infection in pediatrics: a systematic review of Coronavirus disease 2019 (COVID-19) in 850 patients. *Acad Radiol* 2020; 30. doi:10.1016/j.acra.2020.07.031.
- Lu Y, Wen H, Rong D. Clinical characteristics and radiological features of children infected with the 2019 novel Coronavirus. *Clin Radiol* 2020; 75(7):520–525. doi:10.1016/j.crad.2020.04.010.
- Steinberger S, Lin B, Bernheim A, et al. CT features of Coronavirus disease (COVID-19) in 30 pediatric patients. *AJR Am J Roentgenol* 2020; 1–9. doi:10.2214/ajr.20.23145.
- Chen A, Huang J, Liao Y, Liu Z, et al. Differences in clinical and imaging presentation of pediatric patients with COVID-19 in comparison with adults. *Radiology* 2020; 2(2):e200117.
- Liu M, Song Z, Xiao K. High-resolution computed tomography manifestations of 5 pediatric patients with 2019 Novel Coronavirus. *JCAT* 2020; 44(3):311–313. doi:10.1097/rct.0000000000001023.
- Xia W, Shao J, Guo Y, et al. Clinical and CT features in pediatric patients with COVID-19 infection: different points from adults. *Pediatr Pulmonol* 2020; 55(5):1169–1174. doi:10.1002/ppul.24718.
- Hansell DM, Bankier AA, MacMahon H, et al. Fleischner Society: glossary of terms for thoracic imaging. *Radiology* 2008; 246(3):697–722. doi:10.1148/radiol.2462070712.
- Salehi S, Abedi A, Balakrishnan S, et al. Coronavirus disease 2019 (COVID-19) imaging reporting and data system (COVID-RADS) and common lexicon: a proposal based on the imaging data of 37 studies. *Eur Radiol* 2020; 1–13. doi:10.1007/s00330-020-06863-0.
- Prokop M, van Everdingen W, van Rees Vellinga T, et al. CO-RADS - a categorical CT assessment scheme for patients with suspected COVID-19: definition and evaluation. *Radiology* 2020;201473doi:10.1148/radiol.2020201473.
- Simpson S, Kay FU, Abbara S, et al. Radiological Society of North America expert consensus statement on reporting chest CT findings related to COVID-19. Endorsed by the Society of Thoracic Radiology, the J Am Radiol, and RSNA. *Radiology* 2020; 2.2:e200152.
- Carlotti A, Carvalho WB, Johnston C, et al. COVID-19 diagnostic and management protocol for pediatric patients. *Clinics (Sao Paulo)* 2020; 75:e1894. doi:10.6061/clinics/2020/e1894.
- Chen J, Wang XF, Zhang PF. Asymptomatic SARS-CoV-2 infection in children: a clinical analysis of 20 cases. *Zhongguo dang daierke za zhi Chin J Contemp Pediatr* 2020; 22(5):414–418.
- Ma H, Hu J, Tian J, et al. A single-center, retrospective study of COVID-19 features in children: a descriptive investigation. *BMC Med* 2020; 18(1):123. doi:10.1186/s12916-020-01596-9.
- Merkus PJ, Klein WM. Value of Chest CT as COVID 19 screening tool in children. *Eur Respir J* 2020. doi:10.1183/13993003.01241-2020.
- Wong HYF, Lam HYS, Fong AH, et al. Frequency and distribution of chest radiographic findings in COVID-19 positive patients. *Radiology* 2019;201160doi:10.1148/radiol.2020201160.
- Foust AM, Winant AJ, Chu WC, et al. Pediatric SARS, H1N1, MERS, EVALI, and now Coronavirus Disease (COVID-19) pneumonia: what radiologists need to know. *AJR Am J Roentgenol* 2020; 1–9. doi:10.2214/ajr.20.23267.
- Magro C, Mulvey JJ, Berlin D, et al. Complement associated microvascular injury and thrombosis in the pathogenesis of severe COVID-19 infection: a report of five cases. *Transl Res* 2020. doi:10.1016/j.trsl.2020.04.007.
- Feng K, Yun YX, Wang XF, et al. Analysis of CT features of 15 children with 2019 novel Coronavirus infection. *Zhonghuaerke za zhi Chin J Pediatr* 2020; 58(0):E007. doi:10.3760/cma.j.issn.0578-1310.2020.0007.
- Xu Z, Shi L, Wang Y, et al. Pathological findings of COVID-19 associated with acute respiratory distress syndrome. *Lancet Respir Med* 2020; 8(4):20–22.
- Carsana L, Sonzogni A, Nasr A, et al. Pulmonary post-mortem findings in a series of COVID-19 cases from northern Italy: a two-centre descriptive study. *Lancet Infect Dis* 2020. doi:10.1016/S1473-3099(20)30434-5. Jun 8;S1473-3099(20)30434-5.
- Li W, Cui H, Li K, et al. Chest computed tomography in children with COVID-19 respiratory infection. *Pediatr Radiol* 2020; 50(6):796–799. doi:10.1007/s00247-020-04656-7.
- Ma YL, Xia SY, Wang M, et al. Clinical features of children with SARS-CoV-2 infection: an analysis of 115 cases. *Zhongguo dang daierke za zhi Chin J Contemp Pediatr* 2020; 22(4):290–293.
- Zhou Y, Yang GD, Feng K, et al. Clinical features and chest CT findings of coronavirus disease 2019 in infants and young children. *Zhongguo dang daierke za zhi Chin J Contemp Pediatr* 2020; 22(3):215–220.
- Li B, Shen J, Li L, et al. Radiographic and clinical features of children with Coronavirus disease (COVID-19) pneumonia. *Indian Pediatr* 2020; 57(5):423–426. doi:10.1007/s13312-020-1816-8.

SUPPLEMENTARY MATERIALS

Supplementary material associated with this article can be found in the online version at doi:10.1016/j.acra.2020.10.002.